Formation mechanism of bifurcation in mode-locked class-B laser

J. Jahanpanah†, M. Rezazadeh, and A. A. Rahdar

Physics Faculty, Kharazmi University, 49 Mofateh Ave, 15614, Tehran, Iran

(Received 4 April 2014; revised manuscript received 26 May 2014; published online 10 October 2014)

The random oscillations of many longitudinal modes are inevitable in both class –A and –B lasers due to their broadened atomic bandwidths. The destructive superposition of electric field components that are incoherently oscillating at the different longitudinal modes can be converted into a constructive one by using the mode-locking technique. Here, the Maxwell–Bloch equations of motion are solved for a three-mode class-B laser under the mode-locking conditions. The results indicate that the cavity oscillating modes are shifted by changing the laser pumping rate. On the other hand, the frequency components of cavity electric field simultaneously form the various bifurcations. These bifurcations satisfy the well-known mode-locking conditions as well. The atomic population inversion forms only one bifurcation, which is responsible for shaping the cavity electric field bifurcations.

Keywords: bifurcation, multi-mode laser, mode-locking process, ultra-short pulse

PACS: 42.55.Ah, 42.60.Fc, 42.65.Re **DOI:** 10.1088/1674-1056/23/12/124205

1. Introduction

Mode-locking is a well-known technique to synchronize the phase and amplitude of cavity electric field components in frequency domain to produce a train of ultra-short pulses in time domain.[1–3] On the other hand, these synchronizations can be neutralized by the fast fluctuations that are imposed on the laser variables by noise.[4–6] Therefore, the phase modulator (FM) and amplitude modulator (AM) have been used to minimize their irregularities that affect the temporal duration and repetition of pulses in the mode-locking process.[7,8] Currently, various saturable absorbers, such as nonlinear loop mirrors, nonlinear polarization rotation, semiconductor saturable absorber mirrors, carbon nanotubes, and graphene have been employed for ultrafast pulse generation.[9] The effects of hysteresis phenomena on the characteristics of pulses are also investigated in a passively mode-locked fiber laser.[10]

Another important aspect of mode-locking is the formation of bifurcations which have commonly occurred in free-running mode-locked lasers,[11,12] regenerative amplifiers,[13] and injection-locked laser amplifiers.[14,15] The different kinds of saddle-node (SN), Hopf, tongue, and pitchfork bifurcations (optical bistabilities) have vastly been exploited as high speed optical switches,[15,16] optical memories,[17] and flip-flop or optical logics.[18] Recently, the bifurcations have also been observed in vertical cavity surface emitting lasers,[19–21] in two-mode lasers,[22] in quantum dot lasers at pumping currents well above threshold.[23,24]

Here, our main aim is to determine the different bifurcations that may occur for a three-mode class-B laser by solving the Maxwell–Bloch equations of motion. The solutions completely describe the frequency-shift mechanism of modes, and photon distribution between the cavity central mode and two left and right adjacent modes by the different bifurcations. These bifurcations will be shaped only when the damping rate of cavity central mode is different from those of adjacent modes. The perimeter of frequency-shift bifurcations satisfies the mode-locking conditions.[1,25] The bifurcations associated with the left and right adjacent modes may be reciprocal.

On the other hand, the Maxwell–Bloch equations of motion introduce only a single bifurcation for the atomic population inversion. It is turned out that its upper and lower branches are directly corresponding to the upper and lower branches of cavity electric bifurcations. The photon number bifurcations disappear in the below threshold state, where the photon numbers of three oscillating modes simultaneously become negative.

2. Equations of motion and trial solutions

Lasers are generally divided into three important classes of A, B, and C according to the damping rates of cavity electric field γ_C, atomic population inversion $\gamma_{||}$, and atomic dipole moment $\gamma_\perp$ with the relative damping rates $\gamma_\perp \gg \gamma_{||} \gg \gamma_C$, $\gamma_\perp \gg \gamma_{||} \approx \gamma_C$, and $\gamma_\perp \approx \gamma_{||} \approx \gamma_C$ respectively.[1,3,6] The class-B lasers are described by the two important variables of cavity electric field $\alpha(t)$ and atomic population inversion $D(t)$ that obey the Maxwell–Bloch equations of motion in the forms of[26,27]

$$\dot{\alpha} + (\gamma_C + \mathrm{i}\omega_C)\alpha = \frac{\gamma_C}{D_0}(\alpha D) \tag{1}$$

and

$$\dot{D} + \gamma_{||} D = \gamma_{||} D_P - \frac{2\gamma_C}{D_0}|\alpha|^2 D, \tag{2}$$

where ω_C and D_0 are, respectively, the cavity resonance frequency and the static population inversion of single-mode lasers, γ_C and $\gamma_{||}$ are the respective damping rates of variables $\alpha(t)$ and $D(t)$, and $\gamma_{||} D_P$ is the laser pumping rate.[26]

†Corresponding author. E-mail: jahanpanah@khu.ac.ir

© 2014 Chinese Physical Society and IOP Publishing Ltd

A comprehensive trial solution for the cavity electric field $\alpha(t)$, including three different amplitudes $\alpha_{\rm L}$, $\alpha_{\rm C}$, and $\alpha_{\rm R}$ that are simultaneously oscillating in the consecutive left, central, and right modes at the respective frequencies $\omega_{\rm L}=\omega_{\rm C}-\Delta$, $\omega_{\rm C}$, and $\omega_{\rm R}=\omega_{\rm C}+\Delta$, is given by[1]

$$\begin{aligned}\alpha(t) &= \alpha_{\rm L}\exp\left[-{\rm i}(\omega_{\rm L}t+\phi_{\rm L}(t))\right]+\alpha_{\rm C}\exp\left[-{\rm i}(\omega_{\rm C}t+\phi_{\rm C}(t))\right]\\ &\quad+\alpha_{\rm R}\exp\left[-{\rm i}(\omega_{\rm R}t+\phi_{\rm R}(t))\right],\end{aligned}\tag{3}$$

where $\phi_{\rm L}(t)$, $\phi_{\rm C}(t)$, and $\phi_{\rm R}(t)$ are the corresponding temporal phases that impose the following frequency shifts on the cavity modes:

$$\delta_{\rm L}=\frac{{\rm d}\phi_{\rm L}(t)}{{\rm d}t},\quad \delta_{\rm C}=\frac{{\rm d}\phi_{\rm C}(t)}{{\rm d}t},\quad \text{and}\quad \delta_{\rm R}=\frac{{\rm d}\phi_{\rm R}(t)}{{\rm d}t}.\tag{4}$$

The atomic population inversion mimics a similar three-component structure in the form of

$$\begin{aligned}D(t) &= D_0'+D_1\exp\left[-{\rm i}(\Delta t+\phi_D(t))\right]\\ &\quad+D_1^*\exp\left[{\rm i}(\Delta t+\phi_D(t))\right],\end{aligned}\tag{5}$$

where D_0' is the static component of atomic population inversion that supports the amplification of cavity central mode, D_1 and D_1^* are the pulsations produced by the oscillation of adjacent modes with the temporal phase $\phi_{\rm D}(t)$. Similarly, the frequency shift $\delta_{\rm D}={\rm d}\phi_{\rm D}/{\rm d}t$ is also considered for the dynamic components of atomic population inversion. The frequency shifts $\delta_{\rm L}$, $\delta_{\rm C}$, $\delta_{\rm R}$, and $\delta_{\rm D}$ obey the well-known mode-locking relations[1,3,25]

$$2\delta_{\rm C}-\delta_{\rm R}-\delta_{\rm L}=0\tag{6}$$

and

$$2\delta_{\rm D}-\delta_{\rm R}+\delta_{\rm L}=0.\tag{7}$$

Now by substituting the trial solutions (3) and (5) into Eqs. (1) and (2), using the mode-locking conditions (6) and (7), and equating the coefficients of exponential terms that are oscillating at the frequencies $\omega_{\rm L}=\omega_{\rm C}-\Delta$, $\omega_{\rm C}$, and $\omega_{\rm R}=\omega_{\rm C}+\Delta$ on both sides of Eqs. (1) and (2), the following coupled equations are derived for the variables $\alpha_{\rm L}$, $\alpha_{\rm C}$, $\alpha_{\rm R}$, D_1, and $x=D_0'/D_0$ in the forms of[1]

$$(\gamma_{\rm L}-{\rm i}\delta_{\rm L})\,|\alpha_{\rm L}|^2=\gamma_{\rm C}\left(\alpha_{\rm C}\alpha_{\rm L}^*D_1^*/D_0+x|\alpha_{\rm L}|^2\right),\tag{8}$$

$$(\gamma_{\rm C}-{\rm i}\delta_{\rm C})\,|\alpha_{\rm C}|^2=\gamma_{\rm C}\left[\left(\alpha_{\rm L}\alpha_{\rm C}^*D_1+\alpha_{\rm R}\alpha_{\rm C}^*D_1^*\right)/D_0+x|\alpha_{\rm C}|^2\right],\tag{9}$$

$$(\gamma_{\rm R}-{\rm i}\delta_{\rm R})\,|\alpha_{\rm R}|^2=\gamma_{\rm C}\left(\alpha_{\rm C}\alpha_{\rm R}^*D_1/D_0+x|\alpha_{\rm R}|^2\right),\tag{10}$$

$$\begin{aligned}\gamma_{||}D_0' &= \gamma_{||}D_{\rm P}-\frac{2\gamma_{\rm C}}{D_0}\Big[D_0'\left(|\alpha_{\rm C}|^2+|\alpha_{\rm R}|^2+|\alpha_{\rm L}|^2\right)\\ &\quad+D_1\left(\alpha_{\rm C}\alpha_{\rm R}^*+\alpha_{\rm L}\alpha_{\rm C}^*\right)+D_1^*\left(\alpha_{\rm R}\alpha_{\rm C}^*+\alpha_{\rm C}\alpha_{\rm L}^*\right)\Big],\end{aligned}\tag{11}$$

and

$$\begin{aligned}\left[\gamma_{||}-{\rm i}(\Delta+\delta_{\rm D})\right]D_1 &= -\frac{2\gamma_{\rm C}}{D_0}\Big[D_1\left(|\alpha_{\rm C}|^2+|\alpha_{\rm R}|^2+|\alpha_{\rm L}|^2\right)\\ &\quad+D_0'\left(\alpha_{\rm C}\alpha_{\rm L}^*+\alpha_{\rm R}\alpha_{\rm C}^*\right)+D_1^*\alpha_{\rm R}\alpha_{\rm L}^*\Big],\end{aligned}\tag{12}$$

where D_0'/D_0 is the static population inversion ratio of three-mode to single-mode lasers.[1] So far, we have introduced seven equations (6)–(12) for the motion of nine variables $\alpha_{\rm L}$, $\alpha_{\rm C}$, $\alpha_{\rm R}$, x, D_1, $\delta_{\rm L}$, $\delta_{\rm C}$, $\delta_{\rm R}$, and $\delta_{\rm D}$. If the complex conjugates of Eqs. (8) and (10) are substituted into Eq. (9), then the real and imaginary parts of the resultant equation will provide the two required equations in the forms of

$$(1-x)\,|\alpha_{\rm C}|^2=(1+\varepsilon-x)\left(|\alpha_{\rm R}|^2+|\alpha_{\rm L}|^2\right)\tag{13}$$

and

$$-\delta_{\rm C}\,|\alpha_{\rm C}|^2=\delta_{\rm R}\,|\alpha_{\rm R}|^2+\delta_{\rm L}\,|\alpha_{\rm L}|^2,\tag{14}$$

where symmetrical loss coefficient ε plays an adjusting role in damping rates of left and right adjacent modes according to $\gamma_{\rm L}=\gamma_{\rm R}=\gamma_{\rm C}(1+\varepsilon)$. It will be seen that no bifurcation will be formed for the special case of equal damping rates $\gamma_{\rm L}=\gamma_{\rm R}=\gamma_{\rm C}$ $(\varepsilon=0)$ in the following section.

3. Formation mechanism of bifurcations

The simultaneous solutions of Eqs. (6)–(14) are very lengthy and have been given in detail in Ref. [28]. Therefore, we here summarize the main results in terms of variable x, and the two parameters ε and $C'=D_{\rm P}/D_0'$ (the normalized pumping rate of three-mode lasers). There are two unsymmetrical solutions for the frequency shift of adjacent modes $\delta_{\rm R}$ and $\delta_{\rm L}$ in the forms of

$$\delta_{\rm R}=-\delta_{\rm L}\tag{15}$$

and

$$\begin{aligned}\delta_{\rm R} &= -\delta_{\rm L}\\ &= \frac{\gamma_{\rm C}}{\varepsilon}\left[2\varepsilon^3(5-3x)-5\varepsilon^2(1+\varepsilon-x)^2+2\varepsilon(x-1)^3\right]^{1/2},\end{aligned}\tag{16}$$

and two reciprocal solutions with the opposite signs as

$$\begin{aligned}\delta_{\rm R} &= \pm\frac{\gamma_{\rm C}(x-1+\varepsilon)}{\varepsilon(x-1-\varepsilon)}\\ &\quad\times\left[2\varepsilon^3(5-3x)-5\varepsilon^2(1+\varepsilon-x)^2+2\varepsilon(x-1)^3\right]^{1/2}\end{aligned}\tag{17}$$

and

$$\delta_{\rm L}=\mp\frac{\gamma_{\rm C}}{\varepsilon}\left[2\varepsilon^3(5-3x)-5\varepsilon^2(1+\varepsilon-x)^2+2\varepsilon(x-1)^3\right]^{1/2},\tag{18}$$

where solution (15) is exactly the same as Eq. (4.5) in Ref. [29] for the simple case $\varepsilon=0$. The frequency shift of central mode $\delta_{\rm C}$ is evidently zero for the unsymmetrical frequency shifts (15) and (16) according to the mode-locking condition (6). But the non-zero solutions for the frequency shift of cavity central mode $\delta_{\rm C}$ have been determined by substituting the reciprocal relations (17) and (18) into Eq. (6) as

$$\begin{aligned}\delta_{\rm C} &= \mp\frac{\gamma_{\rm C}}{1+\varepsilon-x}\\ &\quad\times\left[2\varepsilon^3(5-3x)-5\varepsilon^2(1+\varepsilon-x)^2+2\varepsilon(x-1)^3\right]^{1/2}.\end{aligned}\tag{19}$$

The normalized number of photons distributed between the cavity central mode $|\alpha_{\rm C}|^2/D_0$ and the right and left adjacent modes $|\alpha_{\rm R}|^2/D_0$ and $|\alpha_{\rm L}|^2/D_0$ is also calculated in the forms of

$$\frac{|\alpha_{\rm C}|^2}{D_0}=\frac{\gamma_{||}(C'-1)}{2\gamma_{\rm C}}\frac{x(1+\varepsilon-x)}{2(1+\varepsilon-x)-\varepsilon x}, \tag{20}$$

$$\frac{|\alpha_{\rm R}|^2}{D_0}=\frac{(x-1)\left[(1+\varepsilon)^2-2(1+\varepsilon)x+x^2+\gamma_{\rm C}^{-2}\delta_{\rm L}^2\right]}{(x-1-\varepsilon)\left[2(1+\varepsilon)^2-4(1+\varepsilon)x+2x^2+\gamma_{\rm C}^{-2}\left(\delta_{\rm R}^2+\delta_{\rm L}^2\right)\right]}\frac{|\alpha_{\rm C}|^2}{D_0}, \tag{21}$$

and

$$\frac{|\alpha_{\rm L}|^2}{D_0}=\frac{(x-1)\left[(1+\varepsilon)^2-2(1+\varepsilon)x+x^2+\gamma_{\rm C}^{-2}\delta_{\rm R}^2\right]}{(x-1-\varepsilon)\left[2(1+\varepsilon)^2-4(1+\varepsilon)x+2x^2+\gamma_{\rm C}^{-2}\left(\delta_{\rm R}^2+\delta_{\rm L}^2\right)\right]}\frac{|\alpha_{\rm C}|^2}{D_0}. \tag{22}$$

For the simpler case $\delta_{\rm R}=-\delta_{\rm L}$, one derives the following solutions that are the same as solutions (5.7) and (5.8) in Ref. [29]:

$$\frac{|\alpha_{\rm R}|^2}{D_0}=\frac{|\alpha_{\rm L}|^2}{D_0}=\frac{1}{2}\frac{|\alpha_{\rm C}|^2}{D_0}=\frac{\gamma_{||}(C'-1)}{4\gamma_{\rm C}}x, \tag{23}$$

by applying the corresponding condition $\varepsilon=0$ to Eqs. (20)–(22).

The frequency shifts of central and adjacent modes simultaneously undertake the acceptable real values in Eqs. (16)–(19), when the variable x satisfies the following inequality

$$2\varepsilon^3(5-3x)-5\varepsilon^2(1+\varepsilon-x)^2+2\varepsilon(x-1)^3\geq 0. \tag{24}$$

Therefore, the normalized minimal population inversion $x_{\rm min}=(D_0'/D_0)_{\rm min}$ can numerically be calculated by zeroing Eq. (24) as plotted in Fig. 1.

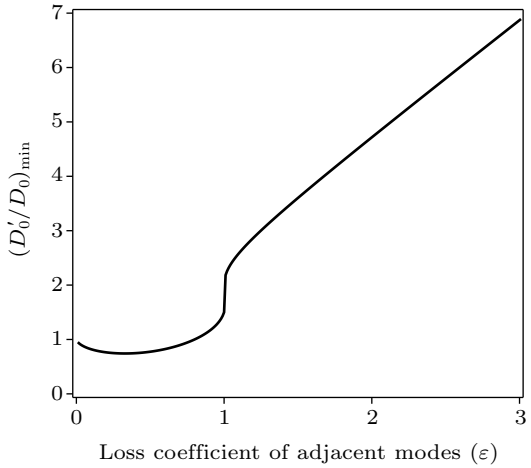


Fig. 1. Minimal atomic population inversion versus parameter ε by zeroing the common terms of frequency shifts $\delta_{\rm R}$, $\delta_{\rm L}$, and $\delta_{\rm C}$ in Eqs. (16)–(19).

Finally, the key variable x obeys a fifteenth-order equation in the form of[28]

$$A_{15}x^{15}+A_{14}x^{14}+\cdots+A_1x+A_0=0, \tag{25}$$

where the coefficients A_i $(i=15,14,\ldots,1,0)$ are very lengthy and each of them is a function of four important parameters C', ε, $\Delta'=\Delta/\gamma_{\rm C}$, and $a=\gamma_{||}/\gamma_{\rm C}$, as given in Appendix A. The numerical solutions of Eq. (25) continuously switch between no real and two real roots (except turning point with one real root) that form a single bifurcation. The variation of normalized population inversion $x=D_0'/D_0$ with normalized pumping rate C' is plotted in Fig. 2 for the typical values $\varepsilon=2$, $\Delta'=20$, and $a=1$. The population inversion bifurcation is apparently composed of the two upper (UB) and lower (LB) branches so that LB intersects the vertical axis at the minimal population inversion $(D_0'/D_0)_{\rm min}=4.7$, which is in complete agreement with its corresponding value in Fig. 1 for $\varepsilon=2$.

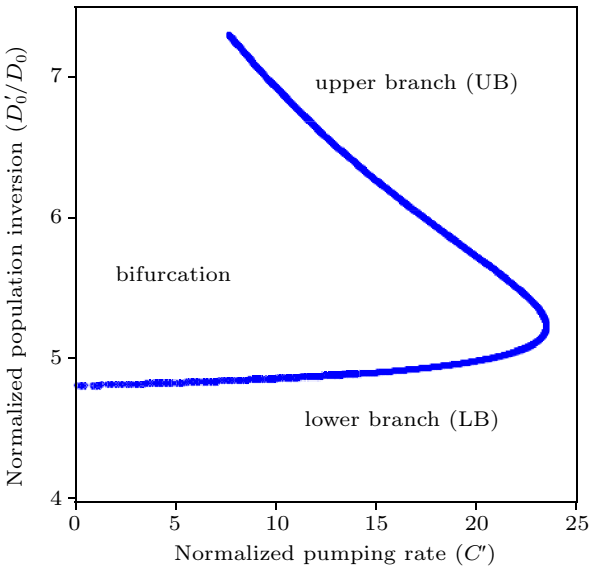


Fig. 2. (color online) Atomic population inversion bifurcation D_0'/D_0 versus normalized pumping rate C' by numerically solving fifteenth-order equation (25) for the typical values $\varepsilon=2$, $\Delta'=20$, and $a=1$.

Now, the normalized frequency shifts of modes $\delta_{\rm R}/\gamma_{\rm C}$, $\delta_{\rm L}/\gamma_{\rm C}$, and $\delta_{\rm C}/\gamma_{\rm C}$ are numerically calculated by substituting the real solutions of Eq. (25) into Eqs. (16)–(19) respectively. The variations of $\delta_{\rm R}/\gamma_{\rm C}$, $\delta_{\rm L}/\gamma_{\rm C}$, and $\delta_{\rm C}/\gamma_{\rm C}$ with normalized pumping rate C' for the typical values $\varepsilon=2$, $\Delta'=20$, and $a=1$ are plotted in Fig. 3(a) for the unsymmetrical case (16), and in Fig. 3(b) for the reciprocal cases (17) and (18). It is seen that the normalized frequency shift of cavity central mode

δ_C/γ_C is always zero in Fig. 3(a), whereas it holds a third bifurcation in Fig. 3(b) due to unequal frequency shifts of adjacent modes in the opposite directions. However, the sum of the normalized frequency shift bifurcations δ_R/γ_C, δ_L/γ_C, and δ_C/γ_C satisfies the well-known condition of mode-locking (6) in both unsymmetrical and reciprocal cases. It should be noticed that the upper branches (UBs) and the lower branches (LBs) of all bifurcations must be separately added to each other to gain the mode-locking condition (6) in Figs. 3(a) and 3(b).

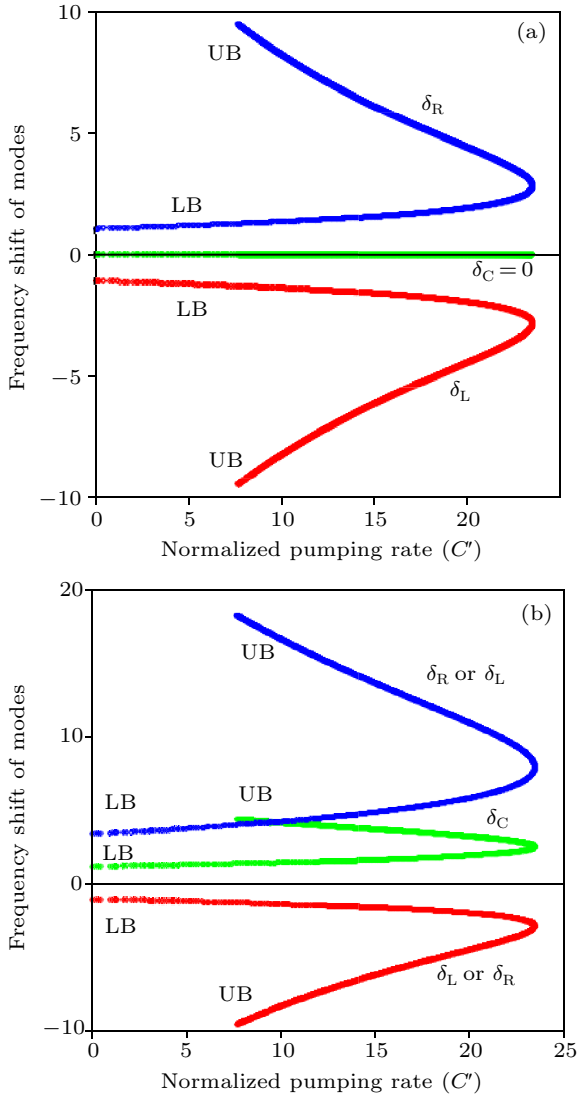


Fig. 3. (color online) Normalized frequency-shift bifurcations δ_R/γ_C, δ_L/γ_C, and δ_C/γ_C versus normalized pumping rate C' for the same typical values chosen in Fig. 2(a) for the unsymmetrical case (16) with $\delta_C = 0$ and (b) for the reciprocal cases (17) and (18) with $\delta_C \neq 0$. The LB and UB of bifurcations individually correspond to each other by the mode-locking condition (6).

The formation mechanism of bifurcations can also be investigated in terms of the normalized frequency separation of cavity modes $\Delta' = \Delta/\gamma_C$ rather than the normalized pumping rate C'. The variations of normalized frequency shifts δ_R/γ_C, δ_L/γ_C, and δ_C/γ_C with Δ' are plotted in Fig. 4 for the typical values $\varepsilon = 2$, $C' = 2$, and $a = 1$. By comparing Fig. 3 with Fig. 4, it is seen that the turning points of bifurcations are reversed by changing the horizontal axis from C' to Δ'. Thus, the turning points are corresponding to the maximal or minimal values for which the mode-locking conditions (6) and (7) hold true.

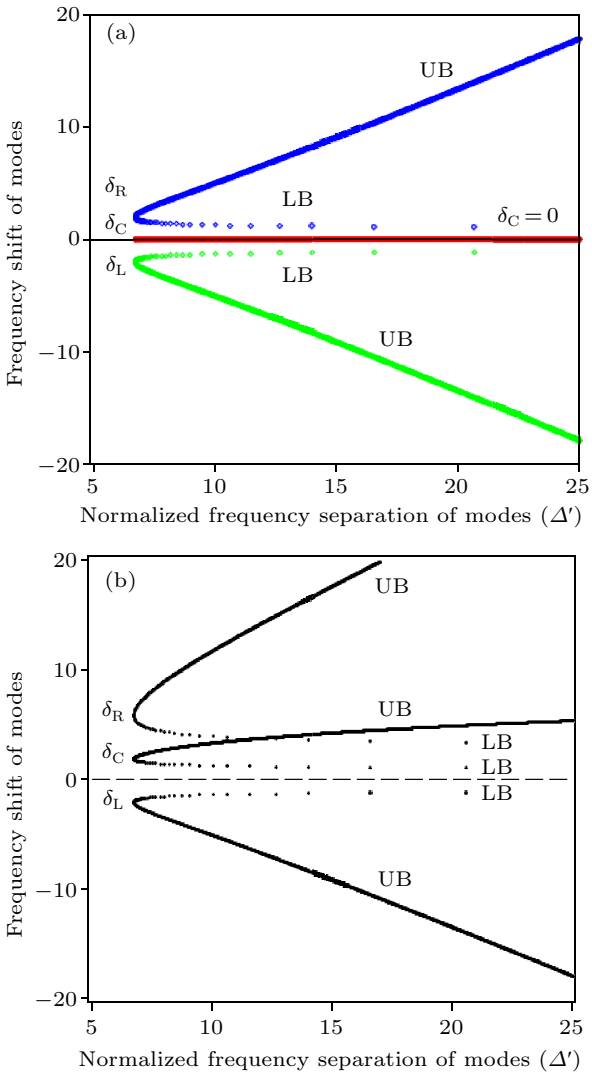


Fig. 4. (color online) The same as Fig. 3, except that the horizontal axis is replaced by the normalized frequency separation of consecutive modes Δ'. The turning points are evidently reversed.

The photon numbers of oscillating modes are now calculated by substituting the real solutions of fifteenth-order equation (25) into Eqs. (20)–(22). The variations of normalized photon numbers $|\alpha_C|^2/D_0$, $|\alpha_R|^2/D_0$, and $|\alpha_L|^2/D_0$ with normalized pumping rate C' are plotted in Fig. 5 by choosing the same typical values $\varepsilon = 2$, $\Delta' = 20$, and $a = 1$; figure 5(a) is for the unsymmetrical frequency shift (16), and figure 5(b) is for the reciprocal frequency shifts (17) and (18). As shown evidently, the photon number bifurcations simultaneously become negative for the normalized pumping rate $C' < 1$ associated with the below-threshold state of three-mode laser.

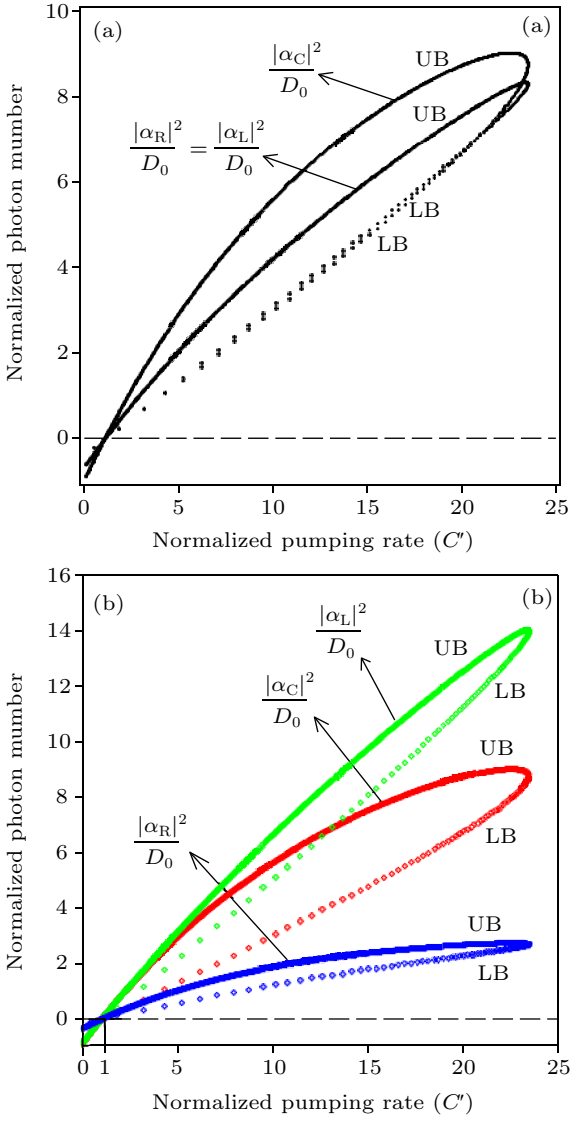


Fig. 5. (color online) Normalized photon number bifurcations of central and adjacent modes versus normalized pumping rate C' for the same typical values as those chosen in Fig. 2(a) for the unsymmetrical case (16) with $|\alpha_R|^2 = |\alpha_L|^2$ and (b) for the reciprocal cases (17) and (18) with $|\alpha_R|^2 \neq |\alpha_L|^2$. The below-threshold state is obviously associated with $C' < 1$, where all three bifurcations become simultaneously negative.

4. Conclusion

The mode-locking features of a three-mode class-B laser are generalized from the simple case $\gamma_R = \gamma_L = \gamma_C$ ($\varepsilon = 0$)[29] to the much complicated symmetrical case $\gamma_R = \gamma_L = \gamma_C(1+\varepsilon)$ ($\varepsilon_R = \varepsilon_L = \varepsilon \neq 0$). In contrast to the former case, the Maxwell–Bloch equations of motion (8)–(14) now demonstrate the much complicated solutions in the form of bifurcations that are in complete agreement with the previous theoretical and experimental results.[11–15]

The cavity electric field bifurcations originate from the atomic population inversion bifurcation. The fifteenth-order equation (25) is numerically solved to describe the motion of static population inversion component D_0'/D_0 in detail. There are only two real solutions that hold a single bifurcation for the atomic population inversion, as indicated in Fig. 2. By substituting these solutions into Eqs. (16)–(22), the corresponding bifurcations are derived for the variables of normalized frequency shifts δ_R/γ_C, δ_L/γ_C, and δ_C/γ_C, and the normalized photon numbers $|\alpha_C|^2/D_0$, $|\alpha_R|^2/D_0$, and $|\alpha_L|^2/D_0$ as shown in Figs. 3–5. So far, we have not seen any reports about the atomic population inversion bifurcation. But, there are many theoretical and experimental results to confirm the frequency (phase) and intensity (amplitude) bifurcations in semiconductor lasers,[19–21] in two-mode lasers,[22] in quantum dot lasers,[23,24] and in optical fiber lasers.[30,31]

The cavity electric field bifurcations are commonly dependent on the four important laser parameters, i.e., normalized pumping rate C', normalized frequency separation of consecutive modes Δ', additional damping coefficient of adjacent modes ε, and damping ratio of atomic population inversion to cavity electric field $a = \gamma_{||}/\gamma_C$. These bifurcations have been widely used in the optical devices.[15–18]

Finally, the stabilities of three oscillating modes are violated, when the photon number bifurcations $|\alpha_C|^2/D_0$, $|\alpha_R|^2/D_0$, and $|\alpha_L|^2/D_0$ simultaneously become negative in the normalized pumping rates $C' < 1$ as shown evidently in Fig. 5. This instability range mimics the instability range of single mode laser for the normalized pumping rates $C < 1$.[26]

Appendix A: Coefficients A_i ($i = 15, 14, \ldots, 1, 0$) of Eq. (25)

The coefficients of fifteenth-order atomic population inversion equation (25) are summarized as follows:

$$A_{15} = 2\varepsilon(\varepsilon+2)^2,$$

$$A_{14} = \varepsilon(-13\varepsilon^3 - 86\varepsilon^2 - 180\varepsilon - 120) + 4a\varepsilon^2(\varepsilon+2)(C'-1),$$

$$A_{13} = 4\varepsilon(9\varepsilon^4 + 88\varepsilon^3 + 298\varepsilon^2 + 420\varepsilon + 210) - 2a\varepsilon^2(15c'\varepsilon^2 + 60c'\varepsilon + 56c' - 17\varepsilon^2 - 68\varepsilon - 64) + 2a^2\varepsilon^3(C'-1)^2,$$

$$A_{12} = -\varepsilon(\varepsilon+2)(67\varepsilon^4 + 662\varepsilon^3 + 2446\varepsilon^2 + 3640\varepsilon + 1820) + a^2\varepsilon^3[-C'^2(17\varepsilon+26) + C'(38\varepsilon+60) - (21\varepsilon+34)]$$
$$+ 2a\varepsilon^2[C'(49\varepsilon^3 + 306\varepsilon^2 + 592\varepsilon + 360) - 2(31\varepsilon^3 + 194\varepsilon^2 + 378\varepsilon + 232] - \Delta'^2\varepsilon^2(\varepsilon+2)^2,$$

$$A_{11} = 2\varepsilon(47\varepsilon^6 + 635\varepsilon^5 + 3612\varepsilon^4 + 11146\varepsilon^3 + 18991\varepsilon^2 + 16380\varepsilon + 5460) + 2\Delta'^2\varepsilon^2(3\varepsilon+4)(\varepsilon+3)(\varepsilon+2)$$
$$+ 2a^2\varepsilon^3[C'^2(32\varepsilon^2 + 100\varepsilon + 76) - C'(79\varepsilon^2 + 256\varepsilon + 200) + 2(24\varepsilon^2 + 80\varepsilon + 64)] - 2a\varepsilon^2[C'(99\varepsilon^4 + 814\varepsilon^3$$

$$+2445\varepsilon^2+3124\varepsilon+1408)-(135\varepsilon^4+1140\varepsilon^3+3471\varepsilon^2+4468\varepsilon+2032)],$$

$$A_{10}=-\varepsilon(79\varepsilon^7+1486\varepsilon^6+10011\varepsilon^5+36828\varepsilon^4+84051\varepsilon^3+115522\varepsilon^2+84084\varepsilon+24024)-\Delta'^2\varepsilon^2(15\varepsilon^4$$
$$+138\varepsilon^3+437\varepsilon^2+572\varepsilon+264)+a^2\varepsilon^3[-2C'^2(72\varepsilon^3+335\varepsilon^2+524\varepsilon+264)+2C'(193\varepsilon^3+946\varepsilon^2$$
$$+763\varepsilon+788)-(255\varepsilon^3+1300\varepsilon^2+2152\varepsilon+1136)]+2a\varepsilon^2[C'(143\varepsilon^5+1400\varepsilon^4+5515\varepsilon^3$$
$$+10904\varepsilon^2+10450\varepsilon+3740)-2(103\varepsilon^5+1056\varepsilon^4+4310\varepsilon^3+8659\varepsilon^2+8349\varepsilon+3014)],$$

$$A_9=4\varepsilon(10\varepsilon^8+263\varepsilon^7+2489\varepsilon^6+11155\varepsilon^5+30109\varepsilon^4+54549\varepsilon^3+63283\varepsilon^2+40040\varepsilon+10010)$$
$$+4\Delta'^2\varepsilon^2(6\varepsilon^5+68\varepsilon^4+299\varepsilon^3+621\varepsilon^2+605\varepsilon+220)+2a^2\varepsilon^3[C'^2(110\varepsilon^4+659\varepsilon^3+1542\varepsilon^2+1612\varepsilon+606)$$
$$-C'(315\varepsilon^4+2030\varepsilon^3+4970\varepsilon^2+5336\varepsilon+2052)+223\varepsilon^4+1521\varepsilon^3+3862\varepsilon^2+4244\varepsilon+1666]$$
$$+4a\varepsilon^2[-C'(145\varepsilon^6+1732\varepsilon^5+8164\varepsilon^4+21022\varepsilon^3+31176\varepsilon^2+24024\varepsilon+7128)+225\varepsilon^6$$
$$+2778\varepsilon^5+13776\varepsilon^4+36850\varepsilon^3+55496\varepsilon^2+42944\varepsilon+12848],$$

$$A_8=\varepsilon(7\varepsilon^9-400\varepsilon^8-5984\varepsilon^7-38048\varepsilon^6-127646\varepsilon^5-270936\varepsilon^4-407484\varepsilon^3-412104\varepsilon^2-231660\varepsilon-51480)$$
$$-\Delta'^2\varepsilon^2(27\varepsilon^7+360\varepsilon^6+1936\varepsilon^4+5480\varepsilon^3+8466\varepsilon^2+6600\varepsilon+1980)+a^2\varepsilon^3[-C'^2(242\varepsilon^5+1730\varepsilon^4$$
$$+5213\varepsilon^3+8200\varepsilon^2+6454\varepsilon+1932)+2C'(367\varepsilon^5+2874\varepsilon^4+9251\varepsilon^3+15144\varepsilon^2+12202\varepsilon+3732)$$
$$-(551\varepsilon^5+4646\varepsilon^4+15781\varepsilon^3+26704\varepsilon^2+21970\varepsilon+6852)+2a\varepsilon^2[C'(93\varepsilon^7+1490\varepsilon^6+8688\varepsilon^5$$
$$+26702\varepsilon^4+51146\varepsilon^3+61164\varepsilon^2+39600\varepsilon+10032)-2(79\varepsilon^7+1296\varepsilon^6+7849\varepsilon^5+25419\varepsilon^4$$
$$+50614\varepsilon^3+61344\varepsilon^2+39798\varepsilon+10164),$$

$$A_7=2\varepsilon(-26\varepsilon^{10}-97\varepsilon^9+922\varepsilon^8+9812\varepsilon^7+46622\varepsilon^6+125066\varepsilon^5+217944\varepsilon^4+280500\varepsilon^3+253407\varepsilon^2$$
$$+128700\varepsilon+25740)+2\Delta'^2\varepsilon^2(7\varepsilon^7+159\varepsilon^6+1074\varepsilon^5+3706\varepsilon^4+7682\varepsilon^3+9498\varepsilon^2+6204\varepsilon+1584)$$
$$+2a^2\varepsilon^3[C'^2(96\varepsilon^6+803\varepsilon^5+2873\varepsilon^4+5824\varepsilon^3+6946\varepsilon^2+4396\varepsilon+1092)-C'(309\varepsilon^6+2866\varepsilon^5$$
$$+11169\varepsilon^4+24058\varepsilon^3+29726\varepsilon^2+19208\varepsilon+4872)+2(123\varepsilon^6+1241\varepsilon^5+5196\varepsilon^4+11771\varepsilon^3$$
$$+14985\varepsilon^2+9866\varepsilon+2550)]+2a\varepsilon^2[-C'(25\varepsilon^8+790e^7+6349\varepsilon^6+24286\varepsilon^5 55148\varepsilon^4+84364\varepsilon^3$$
$$+85218\varepsilon^2+47784\varepsilon+10560)+(53\varepsilon^8+1524\varepsilon^7+12557\varepsilon^6+50008\varepsilon^5+119732\varepsilon^4+190528\varepsilon^3$$
$$+194502\varepsilon^2+109032\varepsilon+24288)],$$

$$A_6=\varepsilon(12\varepsilon^{11}+512\varepsilon^{10}+1217\varepsilon^9-5424\varepsilon^8-41518\varepsilon^7-15972\varepsilon^6-347438\varepsilon^5-511512\varepsilon^4-575619\varepsilon^3-473594\varepsilon^2$$
$$-220220\varepsilon-40040)+\Delta'^2\varepsilon^2(3\varepsilon^8-114\varepsilon^7-1529\varepsilon^6-6944\varepsilon^5-17390\varepsilon^4-28364\varepsilon^3-29442\varepsilon^2-16632\varepsilon-3696)$$
$$+a^2\varepsilon^3[-C'^2(104\varepsilon^7+1050\varepsilon^6+4371\varepsilon^5+10456\varepsilon^4+16095\varepsilon^3+15564\varepsilon^2+8260\varepsilon+1752)+2C'(179\varepsilon^7+2030\varepsilon^6$$
$$+9330\varepsilon^5+24226\varepsilon^4+39455\varepsilon^3+39364\varepsilon^2+21280\varepsilon+4608)-(305\varepsilon^7+3784\varepsilon^6+18902\varepsilon^5+52616\varepsilon^4$$
$$+89821\varepsilon^3+92032\varepsilon^2+50596\varepsilon+11160)]+2a\varepsilon^2[C'(-21\varepsilon^9+152\varepsilon^8+2817\varepsilon^7+14912\varepsilon^6+42266\varepsilon^5$$
$$+75878\varepsilon^4+96950\varepsilon^3+85464\varepsilon^2+42438\varepsilon+8316)+2(12\varepsilon^9-194\varepsilon^8-3118\varepsilon^7$$
$$-17057\varepsilon^6-50369\varepsilon^5-95451\varepsilon^4-126952\varepsilon^3-112698\varepsilon^2-55803\varepsilon-11022)],$$

$$A_5=4\varepsilon(-6\varepsilon^{12}-28\varepsilon^{11}-484\varepsilon^{10}-868\varepsilon^9+2747\varepsilon^8+14882\varepsilon^7+44746\varepsilon^6+86752\varepsilon^5+110043\varepsilon^4+109978\varepsilon^3+83732\varepsilon^2$$
$$+36036\varepsilon+6006)+4\Delta'^2\varepsilon^2(-3\varepsilon^9-15\varepsilon^8+98\varepsilon^7+1014\varepsilon^6+3427\varepsilon^5+6653\varepsilon^4+8932\varepsilon^3+8052\varepsilon^2+4026\varepsilon+792)$$
$$+2a^2\varepsilon^3(\varepsilon+1)[C'^2(17\varepsilon^7+208\varepsilon^6+924\varepsilon^5+2200\varepsilon^4+3432\varepsilon^3+3615\varepsilon^2+2155\varepsilon+489)-C'(63\varepsilon^7+899\varepsilon^6$$
$$+4513\varepsilon^5+11949\varepsilon^4+20210\varepsilon^3+22198\varepsilon^2+13478\varepsilon+3138)+(58\varepsilon^7+923\varepsilon^6+5113\varepsilon^5+14829\varepsilon^4+26858\varepsilon^3$$
$$+30567\varepsilon^2+18883\varepsilon+4497)]+2a\varepsilon^2[C'(28\varepsilon^{10}+156\varepsilon^9-466\varepsilon^8-5498\varepsilon^7-21317\varepsilon^6-47898\varepsilon^5-70870\varepsilon^4$$
$$-77980\varepsilon^3-61479\varepsilon^2-27500\varepsilon-4840)+(-46\varepsilon^{10}-226\varepsilon^9+1326\varepsilon^8+14282\varepsilon^7+57801\varepsilon^6+135208\varepsilon^5$$
$$+211598\varepsilon^4+242668\varepsilon^3+191817\varepsilon^2+85316\varepsilon+15136)],$$

$$A_4=-\varepsilon(20\varepsilon^{13}-144\varepsilon^{12}-420\varepsilon^{11}-3704\varepsilon^{10}-5525\varepsilon^9+15208\varepsilon^8+58792\varepsilon^7+143936\varepsilon^6+248615\varepsilon^5+275436\varepsilon^4$$
$$+247258\varepsilon^3+176596\varepsilon^2+70980\varepsilon+10920)+\Delta'^2\varepsilon^2(12\varepsilon^{10}+112\varepsilon^9+258\varepsilon^8-836\varepsilon^7-6557\varepsilon^6-17384\varepsilon^5$$
$$-27232\varepsilon^4-31016\varepsilon^3-24909\varepsilon^2-11220\varepsilon-1980)+a^2\varepsilon^3(\varepsilon+1)^2[-C'^2(5\varepsilon^7+98\varepsilon^6+522\varepsilon^5+1266\varepsilon^4+1894\varepsilon^3$$

$$+2132\varepsilon^2+1485\varepsilon+362)+2C'(10\varepsilon^7+244\varepsilon^6+1525\varepsilon^5+4222\varepsilon^4+7070\varepsilon^3+8444\varepsilon^2+5967\varepsilon+1502)$$
$$-(20\varepsilon^7+564\varepsilon^6+3969\varepsilon^5+12278\varepsilon^4+22650\varepsilon^3+28444\varepsilon^2+20409\varepsilon+5282)]+2a\varepsilon^2[C'(-10\varepsilon^{11}-152\varepsilon^{10}$$
$$-362\varepsilon^9+866\varepsilon^8+6343\varepsilon^7+19098\varepsilon^6+35552\varepsilon^5+44554\varepsilon^4+43157\varepsilon^3+31026\varepsilon^2+12672\varepsilon+2024)$$
$$+2(10\varepsilon^{11}+150\varepsilon^{10}+333\varepsilon^9-1365\varepsilon^8-10031\varepsilon^7-31854\varepsilon^6-61579\varepsilon^5-81893\varepsilon^4-82855\varepsilon^3$$
$$-59398\varepsilon^2-24046\varepsilon-3872)],$$

$$A_3=2\varepsilon(60\varepsilon^{13}-196\varepsilon^{12}-420\varepsilon^{11}-1894\varepsilon^{10}-2677\varepsilon^9+6966\varepsilon^8+19812\varepsilon^7+39499\varepsilon^6+62563\varepsilon^5+61100\varepsilon^4$$
$$+49666\varepsilon^3+33681\varepsilon^2+12740\varepsilon+1820)+2\Delta'^2\varepsilon^2(\varepsilon+1)(-36\varepsilon^9-138\varepsilon^8+70\varepsilon^7+661\varepsilon^6+2654\varepsilon^5+4496\varepsilon^4$$
$$+4782\varepsilon^3+4373\varepsilon^2+2310\varepsilon+440)+2a^2\varepsilon^3[C'^2(\varepsilon+2)(\varepsilon+1)^3(5\varepsilon^5+32\varepsilon^4+51\varepsilon^3+54\varepsilon^2+66\varepsilon+20)$$
$$-C'(\varepsilon+1)^3(30\varepsilon^6+319\varepsilon^5+1039\varepsilon^4+1641\varepsilon^3+2003\varepsilon^2+1752\varepsilon+480)+2(20\varepsilon^9+618\varepsilon^8+3472\varepsilon^7$$
$$+10450\varepsilon^6+10250\varepsilon^5+14485\varepsilon^4+14644\varepsilon^3+9671\varepsilon^2+3590\varepsilon+550)]+2a\varepsilon^2(\varepsilon+1)[C'(40\varepsilon^{10}+2400\varepsilon^9$$
$$+110\varepsilon^8-1049\varepsilon^7-3265\varepsilon^6-7242\varepsilon^5-9496\varepsilon^4-8601\varepsilon^3-7085\varepsilon^2-3364\varepsilon-576)-(100\varepsilon^{10}+614\varepsilon^9$$
$$+230\varepsilon^8-3725\varepsilon^7-13955\varepsilon^6-31904\varepsilon^5-43584\varepsilon^4-43461\varepsilon^3-35607\varepsilon^2-15564\varepsilon-2864)],$$

$$A_2=\varepsilon(-260\varepsilon^{13}+608\varepsilon^{12}+888\varepsilon^{11}+1928\varepsilon^{10}+3255\varepsilon^9-8032\varepsilon^8-17499\varepsilon^7-28134\varepsilon^6-42135\varepsilon^5-36492\varepsilon^4$$
$$-27005\varepsilon^3-17582\varepsilon^2-6300\varepsilon-840)+\Delta'^2\varepsilon^2(\varepsilon+1)^2(-10\varepsilon^{10}+172\varepsilon^8+144\varepsilon^7-213\varepsilon^6-752\varepsilon^5-2378\varepsilon^4$$
$$-1900\varepsilon^3-1929\varepsilon^2-1276\varepsilon-264)+a^2\varepsilon^3(\varepsilon+1)^4[-C'^2(5\varepsilon^3+5\varepsilon+2)(\varepsilon+2)^2+4C'(15\varepsilon^5+79\varepsilon^4+122\varepsilon^3$$
$$+125\varepsilon^2+153\varepsilon+46)-4(30\varepsilon^5+191\varepsilon^4+351\varepsilon^3+407\varepsilon^2+491\varepsilon+154)]+2a\varepsilon^2(\varepsilon+1)^2[C'(-50\varepsilon^9-116\varepsilon^8$$
$$+149\varepsilon^7+352\varepsilon^6+742\varepsilon^5+1416\varepsilon^4+977\varepsilon^3+928\varepsilon^2+542\varepsilon+100)+2(90\varepsilon^9+216\varepsilon^8-295\varepsilon^7-959\varepsilon^6$$
$$-2551\varepsilon^5-4364\varepsilon^4-3665\varepsilon^3-3467\varepsilon^2-1939\varepsilon-362)],$$

$$A_1=4\varepsilon(\varepsilon+1)(2\varepsilon^4-4\varepsilon^3+\varepsilon^2-2\varepsilon-1)(30\varepsilon^8-32\varepsilon^7-43\varepsilon^6-118\varepsilon^5-302\varepsilon^4-204\varepsilon^3-223\varepsilon^2-150\varepsilon-30)$$
$$+4\Delta'^2\varepsilon^2(\varepsilon+1)^3(2\varepsilon^4-4\varepsilon^3+\varepsilon^2-2\varepsilon-1)(2\varepsilon^5-19\varepsilon^3-10\varepsilon^2-29\varepsilon-12)+4a^2\varepsilon^3(\varepsilon+1)^5[-C'(\varepsilon+2)(5\varepsilon^3+5\varepsilon+2)$$
$$+2(10\varepsilon^4+27\varepsilon^3+17\varepsilon^2+37\varepsilon+13)]+4a\varepsilon^2(\varepsilon+1)^3[C'(\varepsilon+2)(5\varepsilon^3+5\varepsilon+2)(2\varepsilon^4-4\varepsilon^3+\varepsilon^2-2\varepsilon-1)$$
$$-(70\varepsilon^8-4\varepsilon^7-171\varepsilon^6-92\varepsilon^5-640\varepsilon^4-365\varepsilon^3-379\varepsilon^2-276\varepsilon-56)],$$

$$A_0=-4\varepsilon(\varepsilon+1)^2(2\varepsilon^4-4\varepsilon^3+\varepsilon^2-2\varepsilon-1)^2[(5\varepsilon^3+5\varepsilon+2)-4\Delta'^2\varepsilon(\varepsilon+1)^2]-4a\varepsilon^2(\varepsilon+1)^4(5\varepsilon^3+5\varepsilon+2)[a\varepsilon(\varepsilon+1)^2$$
$$-2(2\varepsilon^4-4\varepsilon^3+\varepsilon^2-2\varepsilon-1)].$$

References

[1] Jahanpanah J and Eslami H R 2013 *Opt. Commun.* **293** 102
[2] Paunescu G, Hein J and Sauerbrey R 2004 *Appl. Phys. B* **79** 555
[3] Milonni P W and Eberly J H 2010 *Laser Physics* (USA: John Wiley & Sons)
[4] Ho F T 1985 *IEEE J. Quantum Electron.* **21** 1806
[5] Quinlan F, Gee S, Ozharar S and Delfyett P J 2006 *Opt. Lett.* **31** 2870
[6] Jahanpanah J, Shavandi F and Soleimani A 2013 *Laser Phys.* **23** 55005
[7] Li Y F, Herczfeld P R and Narducci L M 2006 *IEEE J. Quantum Electron.* **42** 525
[8] Paschotta R 2004 *Appl. Phys. B* **79** 163
[9] Liu X M, Han D D, Sun Z P, Zeng C, Lu H, Mao D, Cui Y D and Wang F Q 2013 *Sci. Rep.* **3** 2718
[10] Liu X M 2010 *Phys. Rev. A* **81** 023811
[11] Font J, Vilaseca R, Prati F and Roldan E 2006 *Opt. Commun.* **261** 336
[12] Nguyen B A and Mandel P 1996 *Phys. Rev. A* **54** 1638
[13] Grishin M, Gulbinas V and Michailovas A 2009 *Opt. Express* **17** 15700
[14] Habrusev T, Hegarty S P, Vladimirov A G, Pimenov A, Rachinskii D, Rebrova N, Viktorov E A and Huyet G 2012 *Opt. Express* **20** 25572
[15] Kelleher B, Hegarty S P and Huyet G 2012 *Phys. Rev. E* **86** 066206
[16] Zhukovsky S V, Chigrin D N, Lavrinenko A V and Kroha J 2007 *Phys. Rev. Lett.* **99** 073902
[17] Hill M T, Dorren H J S, Vries T D, Leijtens X J M, Besten J H D, Smalbrugge B, Oei Y S, Binsma H, Khoe G D and Smit M K 2004 *Nature* **432** 206
[18] Raburn M, Takenada M, Takeda K, Song X, Barton J S and Nakano Y 2006 *IEEE Photon. Technol. Lett.* **18** 1421
[19] Gatare I, Sciamanna M, Nizette M, Thienpont H and Panajotov K 2009 *Phys. Rev. E* **80** 026218
[20] Hurtado A, Quirce A, Valle A, Pesquera L and Adams M J 2010 *Opt. Express* **18** 9423
[21] George Pan Z, Jiang S, Dagenais M, Morgan R A, Kojima K, Asom M T, Leibenguth R E, Guth G D and Focht M W 1993 *Appl. Phys. Lett.* **63** 2999
[22] Heinricht P, Wetzel B, O'Brien S, Amann A and Osborne S 2011 *Appl. Phys. Lett.* **99** 11104
[23] Erneux T, Viktorov E A, Kelleher B, Goulding D, Hegarty S P and Huyet G 2010 *Opt. Lett.* **35** 937
[24] Kelleher B, Goulding D, Hegarty S P, Huyet G, Viktorov E A and Erneux T 2012 *in Quantum Dot Devices, Lecture Notes in Nanoscale Science and Technology*, (New York, USA Springer), Vol. 13, p. 1
[25] Ellis J D, Joo K, Buice E S and Spronck J 2010 *Opt. Express* **18** 1373
[26] Jahanpanah J and Loudon R 1996 *Phys. Rev. A* **54** 5210
[27] Siegman A E *Laser* 1986 (Mill Valley: University Science Books)
[28] Rezazadeh M 2013 "The frequency shift determination of three longitudinal modes in class-B lasers" (M. S. Dissertation) (Kharazmi University of Iran) (in Persian)
[29] Jahanpanah J and Rahdar A A 2012 *Opt. Laser Technol.* **44** 2135
[30] Pisarchik A N, Kir'yanov A V, Barmenkov Y O and Jaimes-Reátegui R 2005 *J. Opt. Soc. Am. B* **22** 2107
[31] Pisarchik A N, Barmenkov Y O and Kir'yanov A V 2003 *IEEE J. Quantum Electron.* **39** 1567